Information Systems and E-Business Management vol. 4, PP. 141-160, 2014.
16. Efraim Berkovich, "Search and herding effects in peer-to-peer lending: evidence from prosper. com", Ann. Finance vol. 7, PP. 389–405, 2012.
17. Dawei Shen, Coco Krumme, and Andrew Lippman, Follow the Profit or the Herd? Exploring Social Effects in Peer-to-Peer Lending", The Proceedings of IEEE International Conference on Social Computing, PP. 137-144, 2010.
18. Anna Nagurney, June Dong, and Ding Zhang, "A supply chain network equilibrium model", Transportation Research Part E, vol. 38, PP. 281-303, 2012.
19. Qiang Qiang, Ke Ke, and Yihong Hu, "Finacial networks with socially responsible investing", Computational Management Science vol. 10, PP. 231-352, 2013.
20. Anna Nagurney, A multiproduct network economic model of cybercrime in financial service, Working paper, 2014, University of Massachusetts.

Novel Demosaicking Method Using Nonlocal Similarity Fusion

Guogang WANG [1], Zongliang GAN [1], Guijin TANG [1], Ziguan CUI [1], Jishen LIANG [2], Xiuchang ZHU [1]

[1] Image Process and Image Communication Lab, Nanjing University of Posts and Telecommunications, Nanjing 210003, China
[2] Chongqing Communication Institute,Chongqing 400035, China

Corresponding author is Guogang WANG

Abstract
Although most demosaicking methods assume the existence of high local correlation in estimating the missing color components, such an assumption may fail for images with high color saturation and sharp color transitions. This paper presents a demosaicking scheme by exploiting both the variance of color differences (VCD) and the non-local similarity. First, the missing green components are estimated according to VCD along different edge directions. Then, the nonlocal pixels similar to the estimated pixel are searched to improve the initial estimate of the G channel. Based on the interpolated green plane, the missing blue and red components are preliminarily estimated. Finally, the blue and red channels are enhanced by exploiting nonlocal redundancies respectively. Experimental results show that the proposed algorithm is able to improve the CPSNR, sharpen edge and texture and lead to higher visual quality of reconstructed color images.
Keywords: COLOR DEMOSAICKING, NONLOCAL SIMILARITY, MULTI-COLOR GRADIENT, IMAGE INTERPOLATION

1. Introduction

In the past decades, color image processing has attracted much interest. Digital camera is probably the most popular still image acquisition device, whose commercial proliferation has a great impact on the research in this field. Instead of using three CMOS or CCD sensors, a single sensor based on the Bayer color filter array (CFA) pattern is cost-effective to capture images. In the Bayer CFA-based sensor configuration, only one color is captured at each pixel. In order to reconstruct a full color image, the missing color samples need to be estimated by a process called color demosaicking (CDM). The quality of reconstructed color images depends on the employed demosaicking algorithms and the image contents[1-5].

The early demosaicking methods include nearest-neighbor replication, bilinear interpolation and cubic spline interpolation. Although these classical methods can be simply implemented, they are not able to exploit the information given by the three color components jointly and suffer from many artifacts such as blocking, blurring and zipper effect at edges. Therefore better results are achieved by interpolation approaches specifically designed for the reconstruction of images sampled with a Bayer CFA.

The recently developed methods include the adaptive homogeneity CDM by Hirakawa et al. [6], the successive approximation based CDM by Li [7], the directional linear minimum mean square-error estimation (DLMMSE) based CDM method by Zhang et al. [8], the variance of color-difference based CDM method by Chung et al. [9], and the nonlocal means based self-similarity driven (SSD) method by Buades et al. [10], etc.

Although the Kodak dataset [11,12] has been widely used as a benchmark dataset in evaluating CDM algorithms, it was not originally released for CDM. It has been pointed out in [13] that images in the Kodak dataset have much higher spectral correlation, smaller chromatic gradients and lower color saturation than images in McMaster dataset [14]. Furthermore, compared with the digital color images captured by current digital cameras, the images in Kodak dataset are less saturated and smoother, and hence they are less representative for the applications such as CDM.

Most of the existing demosaicking methods assume high local correlations[13,15]. Such an assumption, however, may be invalid for images such as those in the McMaster dataset. In natural images the correlation is often weak around object boundaries. Consequently, many CDM algorithms derived under the assumption of high correlation may fail in areas of edges.

To improve the demosaicing results for images with lower local redundancy, the paper has proposed a demosaicing method by exploiting effectively both the variance of the color differences and the nonlocal redundancy. First, missing green components are estimated using VCD along different edge directions. Second, according to the similar degree and the non-smooth operator, the image patches are adaptively selected to enhance the local estimate of G channel. Third, the missing B and R components are preliminarily estimated with the help of G channel. Finally, the B and R channels are enhanced by using nonlocal correlations respectively.

The remainder of this paper is organized as follows. Section 2 introduces the details of the proposed VCD-NS algorithm. Simulation results including complexity analysis and image quality evaluation are shown in section 3. Finally, conclusions are drawn in Section 4.

2. The Proposed Demosaicking Algorithm

2.1. Strategy and Flowchart

Figure 1. illustrates the flowchart of the proposed demosaicking algorithm. First, missing green samples are estimated using VCD in a raster scan manner. Second, the nonlocal similarity (NS) is applied to enhance the interpolated G channel. In the third step, the B and R channels are initially interpolated by the aid of the reconstructed G channel. Finally, NS is exploited to enhance the B and R channels.

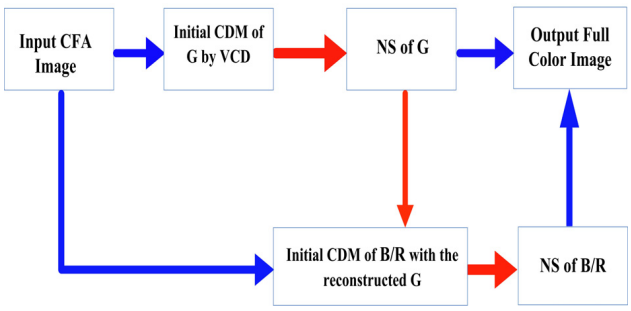

Figure 1. Flowchart of the proposed demosaicking method

One key problem in the initial demosaicking is the usage of local and directional information. The preservation of edges is considerable to the visual quality of reconstructed color images. Since edges usually have one or more dominant directions, the interpolation should be along, instead of across, the edge main directions. With the above considerations, the proposed VCD scheme (the detailed description of VCD is in Section 2.2) puts its focus on how to effectively determine the interpolation direction for estimating a missing green component in edge regions and texture regions. In particular, VCD is used as a supplemen-

tary criterion to determine the interpolation direction for the green components.

2.2. CFA Interpolation Using VCD

As far as a missing green sample in the Bayer CFA is concerned, its neighborhood should be in a form shown in either Figure 2a or Figure 2b. Without loss of generality, only the case shown in Figure 2a is considered. For the other case, the same treatment can be done to estimate the missing green samples by exchanging the roles of the blue samples and the red samples.

In Figure 2a, the center pixel $p_{i,j}$ is represented by $(r_{i,j}, g_{i,j}, B_{i,j})$, where $g_{i,j}$ is the missing G sample

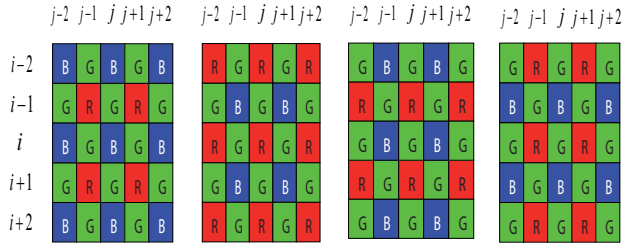

Figure 2. Four 5×5 regions of Bayer CFA pattern having their centers at (a) blue, (b) red, (c)-(d) green CFA samples

needed to be estimated. In this case, the vertical gradient ∇_v and the horizontal gradient ∇_h at position (i, j) are computed as follows.

$$\nabla_v = \sum_{m=0,\pm2}\left[\left|B_{i-2,j+m} - B_{i,j+m}\right| + \left|G_{i-1,j+m} - G_{i+1,j+m}\right| + \left|B_{i,j+m} - B_{i+2,j+m}\right|\right]$$
$$+ \sum_{m=\pm1}\left[\left|G_{i-2,j+m} - G_{i,j+m}\right| + \left|R_{i-1,j+m} - R_{i+1,j+m}\right| + \left|G_{i,j+m} - G_{i+2,j+m}\right|\right] \quad (1)$$

$$\nabla_h = \sum_{m=0,\pm2}\left[\left|B_{i+m,j-2} - B_{i+m,j}\right| + \left|G_{i+m,j-1} - G_{i+m,j+1}\right| + \left|B_{i+m,j} - B_{i+m,j+2}\right|\right]$$
$$+ \sum_{m=\pm1}\left[\left|G_{i+m,j-2} - G_{i+m,j}\right| + \left|R_{i+m,j-1} - R_{i+m,j+1}\right| + \left|G_{i+m,j} - G_{i+m,j+2}\right|\right] \quad (2)$$

∇_v and ∇_h are used to estimate whether there is sharp vertical or horizontal gradient change in the 5×5 window with (i, j) as the center. The non-smooth operator, which is also referred to as non-smooth degree, is defined as follows:

$$e = \max\left(\frac{\nabla_h + \eta}{\nabla_v + \eta}, \frac{\nabla_v + \eta}{\nabla_h + \eta}\right) \quad (3)$$

Where η is a sufficiently small positive number. The smaller is the non-smooth operator, the stronger is the correlation among neighborhood pixels, and vice versa.

The blocks are defined to be the flat blocks if $e < T_2$, where T_2 is a preset threshold value.

It has been found that the color differences of pixels are more or less the same in a local region of a natural image[6]. As a consequence, the variance of color differences can be used to determine the interpolation direction for the G samples.

In the proposed algorithm, the 5×5 block of interest is extended into a 7×7 block by including more neighbors to compute the color differences of the pixels along the axis within the 7×7 window. The VCD of the pixels along the horizontal axis of the 7×7 block, say vcd_h, is defined as

$$vcd_h = \frac{1}{7}\sum_{n\in\varphi}(d_{i,j+n} - \frac{1}{7}\sum_{k\in\varphi} d_{i,j+k})^2 \quad (4)$$

Where $\varphi = \{0, \pm1, \pm2, \pm3\}$ is a set of indexes and $d_{i,j}$ is the color difference of pixel (i, j) which helps to identify a pixel in the 7×7 window. The values of $d_{i,j+n}$ for $n \in \varphi$ can be pre-evaluated, and they are determined sequentially as follows.

$$d_{i,j+n} = B_{i,j+n} - \hat{g}_{i,j+n} \ (n = 0, \pm2) \quad (5)$$

$$d_{i,j+3} = B_{i,j+2} - G_{i,j+3},\ d_{i,j-3} = B_{i,j-2} - G_{i,j-3} \quad (6)$$

$$d_{i,j+m} = (d_{i,j+m-1} + d_{i,j+m+1})/2 \ (m = \pm1) \quad (7)$$

Let vcd_v be the variance of the color differences of the pixels along the vertical axis of the 7×7 block. In particular, it is defined as

$$vcd_v = \frac{1}{7}\sum_{n\in\varphi}(d_{i+n,j} - \frac{1}{7}\sum_{k\in\varphi} d_{i+k,j})^2 \quad (8)$$

Where $\varphi = \{0, \pm1, \pm2, \pm3\}$ is a set of indexes and $d_{i,j}$ is the color difference of pixel (i, j). The values of $d_{i+n,j}$ for $n \in \varphi$ should be pre-evaluated, and they are determined sequentially as follows.

$$d_{i+n,j} = B_{i+n,j} - \hat{g}_{i+n,j} \ (n = 0, \pm2) \quad (9)$$

$$d_{i+3,j} = B_{i+2,j} - G_{i+3,j},\ d_{i-3,j} = B_{i-2,j} - G_{i-3,j} \quad (10)$$

$$d_{i+m,j} = (d_{i+m-1,j} + d_{i+m+1,j})/2 \ (m = \pm1) \quad (11)$$

Since the missing green components are estimated in a raster scan fashion, the final estimates of the green components in position $\Omega_{i,j}$={(i,j-2),(i-2,j)} are

already evaluated. As far as the missing G samples of the pixels in position $\{(i,j+n),(i+n,j)|n=0,2\}$, their preliminary estimates $\hat{g}_{i,j+n}$ and $\hat{g}_{i+n,j}$ have to be evaluated. Concretely, $\hat{g}_{i,j+n}$ is computed with eqn.(12) while $\hat{g}_{i+n,j}$ is determined with eqn.(13). Note the $d_{i,j}$ involved in (4) uses the $\hat{g}_{i,j}$ computed with eqn. (12) while the $d_{i,j}$ involved in eqn.(8) uses the $\hat{g}_{i,j}$ computed with eqn.(13).

$$\hat{g}_{i,j} = \frac{(G_{i,j-1}+G_{i,j+1})}{2} + \frac{(2B_{i,j}-B_{i,j-2}-B_{i,j+2})}{4} \quad (12)$$

$$\hat{g}_{i,j} = \frac{(G_{i-1,j}+G_{i+1,j})}{2} + \frac{(2B_{i,j}-B_{i-2,j}-B_{i+2,j})}{4} \quad (13)$$

Let vcd_d be the variance of the color differences of the diagonal pixels in the 7×7 window. In particular, it is defined by:

$$vcd_d = \frac{1}{2}\left(\frac{1}{7}\sum_{n\in\varphi}(d_{i,j+n} - \frac{1}{7}\sum_{k\in\varphi} d_{i,j+k})^2 + \frac{1}{7}\sum_{n\in\varphi}(d_{i+n,j} - \frac{1}{7}\sum_{k\in\varphi} d_{i+k,j})^2\right) \quad (14)$$

Although the same set of (5)-(7) and (9)-(11) are used to get the $d_{i,j}$ required in the computation of vcd_d, the initial estimates $\hat{g}_{i,j+n}$ and $\hat{g}_{i+n,j}$ involved in these equations are determined by (15).

$$\hat{g}_{i,j} = \frac{(G_{i,j-1}+G_{i,j+1}+G_{i-1,j}+G_{i+1,j})}{4} + \frac{(4B_{i,j}-B_{i,j-2}-B_{i,j+2}-B_{i-2,j}-B_{i+2,j})}{8} \quad (15)$$

The interpolation direction, which offers the minimum variance of color difference, is determined by vcd_h, vcd_v and vcd_d to estimate the missing green component at $(r_{i,j}, g_{i,j}, B_{i,j})$. $g_{i,j}$ is then evaluated using formulation (12), (13) or (15) as follows.

$$\hat{g}_{i,j} = \begin{cases} computation \quad result \quad of \quad (12) & if \quad vcd_h = \min(vcd_h, vcd_v, vcd_d) \\ computation \quad result \quad of \quad (13) & if \quad vcd_v = \min(vcd_h, vcd_v, vcd_d) \\ computation \quad result \quad of \quad (15) & if \quad vcd_d = \min(vcd_h, vcd_v, vcd_d) \end{cases} \quad (16)$$

The blocks which are not classified to be flat blocks are considered to be in an edge regions or a pattern regions. The complexity of the realization of eqn.(4)-(16) is large. In this case, interpolating missing components by eqns. (17) can provide a good demosacing result and save a lot of effort at the same time.

$$\hat{g}_{i,j} = \begin{cases} computation \quad result \quad of \quad (12) & if \quad \nabla_h < \nabla_v \\ computation \quad result \quad of \quad (13) & if \quad \nabla_h > \nabla_v \end{cases} \quad (17)$$

Once the missing G sample is obtained, the same process is used for evaluating the next missing green component in a raster scan manner. In order to evaluate the missing green component in the case shown in Figure 2b, the blue samples can be replaced by the corresponding red samples and the procedures above are followed to determine its interpolation direction and its interpolated value.

2.3. Non-local Enhancement of G Channel

An initial estimate of each missing green sample can be obtained by using the method described in section 2.2. The interpolation may be inaccurate, especially around object boundaries, because only the local correlations in a compact local window is exploited. Luckily, there are many similar structures or patterns in natural images, while a similar structure to the given one may appear far from it. Such nonlocal similarity can be used in image processing [16-24].

To measure the similarity between two given pixels, the similar degree is defined by

$$sd(N_i, N_j) = \frac{1}{1+c\times d(i,j)} \quad (18)$$

Where $d(i,j) = \left\|x(N_i) - x(N_j)\right\|_2^2$, $x(N_i)=\{x(k), k\in N_i\}$, $x(N_j)=\{x(k), k\in N_j\}$, $j=1,2,...,M$, c is a constant and is set as 0.01, M is the total number of the image blocks compared.

We use the nonlocal similarity to enhance the CDM results in this section. For this purpose, similar pixels are searched to the given $\hat{g}_{i,j}$ in the preliminarily recovered G image. Although the searching can be performed in the whole image, this is computationally infeasible. In practice, we search for similar pixels to $\hat{g}_{i,j}$ in a enough large window, which centers on $\hat{g}_{i,j}$ and is denoted by Ω. The block based method can be used to determine the similarity between $\hat{g}_{i,j}$ and other pixels in Ω. Denote by N_i the 5×5 patch centered on the estimated pixel ($\hat{g}_{i,j}$). The N most similar 5×5 image blocks to N_i (including N_i itself), which are denoted by $N_l, l=1,2,\cdots,N$, are searched in Ω. Let e_{N_l} be the non-smooth degree of the image block N_l. To adaptively process the N

most similar image blocks, this detection mechanism is taken as follows:

(1) If $sd(N_i, N_l) < T_1$, then N_l is replaced by N_i;

(2) If $sd(N_i, N_l) \geq T_1$ and $e_{N_l} \geq T_2$, then N_l is replaced by N_i;

(3) N_l is selected in other cases.

For the convenience of expression, we denote the missing G(B, R) component by $g_{i,j}(b_{i,j}, r_{i,j})$, the initial estimate of $g_{i,j}(b_{i,j}, r_{i,j})$ by $\hat{g}^{(1)}_{i,j}(\hat{b}^{(1)}_{i,j}, \hat{r}^{(1)}_{i,j})$, the ultimate estimate of $g_{i,j}(b_{i,j}, r_{i,j})$ by $\hat{G}_{i,j}(\hat{B}_{i,j}, \hat{R}_{i,j})$, and the searched and adaptively processed N most similar pixels to $g_{i,j}(b_{i,j}, r_{i,j})$ by $\hat{g}^{(l)}_{i,j}(\hat{b}^{(l)}_{i,j}, \hat{r}^{(l)}_{i,j}), l = 1, 2, \cdots, N$. $\hat{G}_{i,j}$ can be denoted by the nonlocal enhancement output of $\hat{g}^{(1)}_{i,j}$. Namely, $\hat{G}_{i,j}$ is computed as the weighted average of $\hat{g}^{(l)}_{i,j}$:

$$\hat{G}_{i,j} = \sum_{l=1}^{N} \omega^{(l)} \hat{g}^{(l)}_{i,j} \tag{19}$$

Where the weights $\omega^{(l)}$ are set as $\omega^{(l)} = sd(N_i, N_l)/C$ with $C = \sum_{l=1}^{N} sd(N_i, N_l)$ being the normalization factor to make the sum of $\omega^{(l)}$ be 1.

2.4. Initial Interpolation of B and Rchannels

After interpolating all missing green components of the image, the missing blue and red components are estimated. Figure 2a and Figure 2b show all possible cases where the pixel of interest is located at the center of a 5×5 block. For the case in Figure 2a, the missing red sample of the center, $r_{i,j}$, is obtained by

$$\hat{r}_{i,j} = \hat{G}_{i,j} + \frac{1}{4} \sum_{m=\pm1} \sum_{n=\pm1} (R_{i+m,j+n} - \hat{G}_{i+m,j+n}) \tag{20}$$

As for the case shown in Figure 2b, the missing blue sample of the center, $b_{i,j}$, is obtained by

$$\hat{b}_{i,j} = \hat{G}_{i,j} + \frac{1}{4} \sum_{m=\pm1} \sum_{n=\pm1} (B_{i+m,j+n} - \hat{G}_{i+m,j+n}) \tag{21}$$

Figure 2c and Figure 2d show the two possible cases where a green CFA sample lies in the center of a 5×5 window. For the case shown in Figure 2c, the missing components of the center are obtained by

$$\hat{b}_{i,j} = G_{i,j} + \frac{(B_{i,j-1} - \hat{G}_{i,j-1} + B_{i,j+1} - \hat{G}_{i,j+1})}{2} \tag{22}$$

$$\hat{r}_{i,j} = G_{i,j} + \frac{(R_{i-1,j} - \hat{G}_{i-1,j} + R_{i+1,j} - \hat{G}_{i+1,j})}{2} \tag{23}$$

As for the case in Figure 2d, the missing components of the center are obtained by

$$\hat{b}_{i,j} = G_{i,j} + \frac{(B_{i-1,j} - \hat{G}_{i-1,j} + B_{i+1,j} - \hat{G}_{i+1,j})}{2} \tag{24}$$

$$\hat{r}_{i,j} = G_{i,j} + \frac{(R_{i,j-1} - \hat{G}_{i,j-1} + R_{i,j+1} - \hat{G}_{i,j+1})}{2} \tag{25}$$

2.5. Nonlocal Enhancement of B and R Channels

Once the R and B channels are interpolated with the aid of nonlocally strengthened G channel, they can then be enhanced by utilizing nonlocal correlations in B and R channels respectively. The process is the same as that for the G channel. Namely, $\hat{B}_{i,j}(\hat{R}_{i,j})$ can be computed as the weighted average of $\hat{b}^{(l)}_{i,j}(\hat{r}^{(l)}_{i,j}), l = 2, 3, \cdots, N$.

3. Experimental Results

The performance of various CDM schemes is evaluated on the McMaster dataset. A set of testing images are generated by the 12 McMaster color images in Figure 3. CPSNR [9] is used to measure and quantify the performance of the CDM methods.

Figure 3. 500 × 500 McMaster images used in the experiments. From left to right and top to bottom, these images are labeled as 1 to 12

We denote by VCD-NS the proposed CDM algorithm. The following state-of-the-art CDM algorithms are used to compare: the self-similarity driven (SSD) method [10], the VCD method [9], the adaptive homogeneity-directed (AHD) method [6], the DLMMSE method [8], and the successive approximation (SA) method [7].

In our implementation of VCD-NS, 35 5×5 similar patches are searched in a 37× 37 local window. The thresholds T_1 and T_2 are respectively set as 0.95 and 1.5.

In our experiments, the original color images is down-sampled into Bayer CFA images, and then the full color images are reconstructed using the six algorithms. The CPSNR performance of the six methods are shown in table 1. Among the tested methods, the proposed VCD-NS method obtains the best average performance.

Figure 4 to 6 show the cropped and zoomed demosaicking results of the six algorithms on images 1, 6 and 8. It can be found that the proposed algorithm yields much better demosaicking outputs than the other five algorithms.

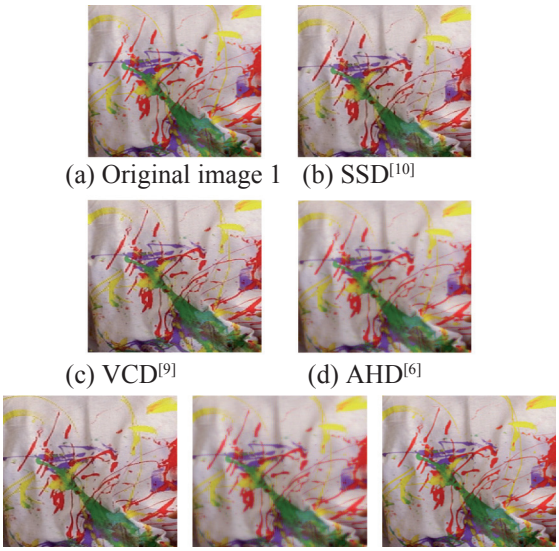

(a) Original image 1 (b) SSD[10] (c) VCD[9] (d) AHD[6] (e) DLMMSE[8] (f) SA[7] (g) VCD-NS

Figure 4. Part of the demosaicing results of Image 1 by different methods

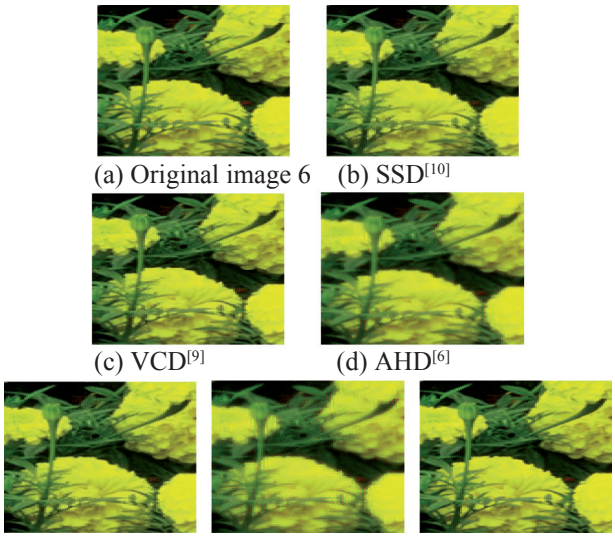

(a) Original image 6 (b) SSD[10] (c) VCD[9] (d) AHD[6] (e) DLMMSE[8] (f) SA[7] (g) VCD-NS

Figure 5. Part of the demosaicing results of Image 6 by different methods

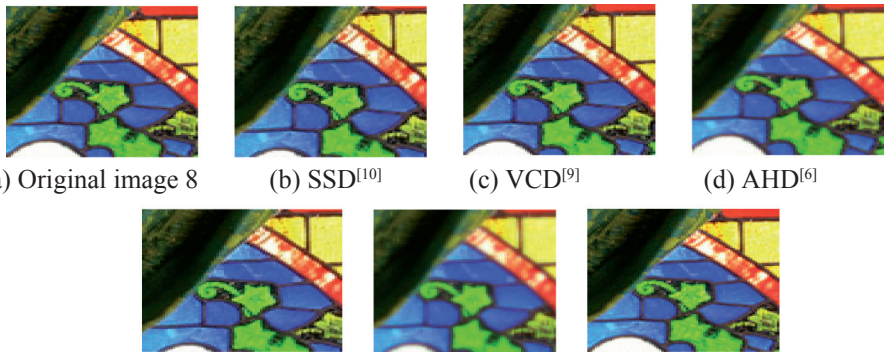

(a) Original image 8 (b) SSD[10] (c) VCD[9] (d) AHD[6] (e) DLMMSE[8] (f) SA[7] (g) VCD-NS

Figure 6. Part of the demosaicing results of Image 8 by different method

The CDM algorithms VCD, AHD, DLMMSE and SA produce many false colors and zipper effects. It is because that they assume smooth color differences but the hypothesis does not hold well on the McMaster dataset. Although the SSD exploits the nonlocal redundancy to recover the color information, it is not effective in using the image local directional information. As a result, SSD still produce many visible color artifacts. The proposed VCD-NS exploits effectively the edge direction information and the image local redundancy, and exploits the nonlocal redundancy to enhance the CDM output. It recovers more faithfully the missing color samples, reducing significantly the color demosaicking errors and artifacts than SSD. Its higher CPSNR in Table 1 also validate their powerful capability in color reproduction.

Similar patch searching, which is one of the main sources of computational cost, is involved in SSD and VCD-NS methods. Therefore, SSD and VCD-NS methods have higher complexity than the local methods VCD, AHD, DLMMSE and SA. Since the complexity of the realization of eqn. (16) and its preparation work(eqns. (4)-(11) and (14)) is large, the proposed VCD-NS algorithm has higher complexity than SSD.

4. Conclusion

An adaptive demosaicing scheme, which exploits effectively both the variance of color differences and the nonlocal redundancy, is presented in this paper. First, initial interpolations of the green channel are obtained based on the variances of the color differences along different edge directions. Second, the non-local redundancy is applied to enhance the interpolated G channel. In the third step, the red and blue channels are initially interpolated with the help of the reconstructed G channel. Finally, nonlocal similarity

Table 1. CPSNR (dB) results using different demosaicking algorithms on the McMaster datase

Images	SSD[10]	VCD[9]	AHD[6]	DLMMSE[8]	SA[7]	VCD-NS
1	31.87	31.65	31.01	31.62	29.22	33.12
2	37.84	37.31	36.73	37.36	35.87	38.29
3	37.01	35.77	36.64	36.86	36.13	37.50
4	39.91	39.11	38.76	39.36	38.17	39.97
5	37.14	36.36	36.01	36.49	34.99	37.55
6	31.24	30.98	30.05	30.67	27.41	32.43
7	34.33	33.34	33.64	34.15	32.12	33.97
8	27.38	26.79	26.63	27.13	23.58	27.79
9	30.51	30.28	28.63	29.60	25.70	31.82
10	35.66	34.73	34.51	34.85	32.36	36.07
11	37.98	37.43	37.43	37.70	36.69	37.69
12	35.14	35.06	33.87	34.92	31.29	37.58
Average	34.67	34.07	33.66	34.23	31.96	35.32

is applied to the R and B channels so that the whole CDM is completed. The VCD-NS algorithm has been tested on the McMaster dataset, and experimental results suggest that the proposed method is able to produce a better objectively and subjectively CDM results as compared with a number of state-of-the-art CDM methods.

References

1. D. B. Conkey and R. Piestun. Color image projection through a strongly scattering wall [J]. Opt Express, 20(25): 27312-27318, 2012.
2. J. Sun and M. F. Tappen. Separable Markov Random Field Model and Its Applications in Low Level Vision [J]. IEEE Transactions on Image Processing, 22(1):402-408, 2013.
3. S. L. Chen and H. R. Chang. Fully pipelined low-cost and high-quality color demosaicking VLSI design for real-time video applications [J]. IEEE Transactions on Circuits and Systems li-express briefs, 62(6): 588-592, 2015.
4. C. Bai, J Li, Z. Lin, J Yu and Y. W. Chen. Penrose demosaicking [J]. IEEE Transactions on Image Processing, 24 (5): 1672-1684, 2015.
5. X. F. Jia, B. T. Zhao, M. R. Zhou and Z. Q. Chen. An edge-adaptive demosaicking method based on image correlation [J]. Journal of Central South University, 22(4): 1397-1404, 2015.
6. K. Hirakawa and T. W. Parks. Adaptive homogeneity-directed demosaicing algorithm [J]. IEEE Transactions on Image Processing, 14(3):360-369, 2005.
7. X. Li. Demosaicing by successive approximation [J]. IEEE Transactions on Image Processing, 2005, 14(3):370-379.
8. L. Zhang and X. Wu. Color demosaicking via directional linear minimum mean square-error estimation [J]. IEEE Transactions on Image Processing, 14(12):2167-2178, 2005.
9. K. -H. Chung and Y. -H. Chan. Color demosaicing using variance of color differences [J]. IEEE Transactions on Image Processing, 15(10):2944-2955, 2006.
10. A. Buades, B. Coll, J. M. Morel, and C. Sbert. Self-similarity driven color demosaicking [J]. IEEE Transactions on Image Processing, 18(6):1192-1202, 2009.
11. L. Fang, O. C. Au, Y. Chen, A. K. Katsaggelos, H. L. Wang and X. Wen. Joint demosaicing and subpixel-based down-sampling for Bayer images: a fast frequency-domain analysis approach [J]. IEEE Transactions on Multimedia, 14(4): 1359-1369, 2012.
12. Kodak color image dataset, http://r0k. us/graphics/kodak/.
13. F. Zhang, X. Wu, X. Yang, W. Zhang and L. Zhang. Robust color demosaicking with adaptation to varying spectral correlation [J]. IEEE Transactions on Image Processing, 18(12): 2706-2717, 2009.
14. L. Zhang, X. L. Wu, A. Buades and X. Li. Color demosaicking by local directional interpolation and nonlocal adaptive thresholding [J]. Journal of electronic imaging, 20(2): 1-29, 2011.
15. Xin Li, B. Gunturk, L. Zhang. Image demosaicking: a systematic survey [C]. Visual Communications and Image Processing, VCIP 2008, 2008.
16. X. D. Zhang, X. CH. Feng and W. W. Wang. Two-Direction Nonlocal Model for Image Denoising [J]. IEEE Transactions on Image Processing, 22(1): 408-412, 2013.

17. W. SH. Dong, L Zhang, G. M. Shi and X. Li. Nonlocally centralized sparse representation for image restoration [J]. IEEE Transactions on Image Processing, 22(4): 1620-1630, 2013.
18. Parrilli, S, Poderico, M, Angelino, C. V. ; Verdoliva, L. A. Nonlocal SAR Image Denoising Algorithm Based on LLMMSE Wavelet Shrinkage [J]. IEEE Transactions on Geoscience and Remote Sensing. 2012, 50(2):606-616.
19. Chul Lee; Chulwoo Lee; Chang-Su Kim. MMSE nonlocal means denoising algorithm for Poisson noise removal [C]. In Proceedings of 18th IEEE International Conference on Image Processing, Page(s): 2561 –2564, 2011.
20. Iqbal M Z, Ghafoor A, Siddiqui A M. Satellite Image Resolution Enhancement Using Dual-Tree Complex Wavelet Transform And Nonlocal Means [J]. IEEE Geoscience and Remote Sensing Letters, 2013, 10(3), 451-455.
21. Chaudhury K N, Acceleration of the Shiftable O(1) Algorithm for Bilateral Filtering and Nonlocal Means [J]. IEEE transactions on image processing, 2013, 22(4), 1291-1300.
22. K. Zhang, H. Li, S. Yang, M. Wang, Z. Liu, R. Qu and L. Jiao. Sparse double-geometric nonlocal mean image recovery via steerable kernel [J]. Applied Soft Computing, 2015, 33: 77-85.
23. F. Chen, X. Zeng and M. Wang. Image denoising via local and nonlocal circulant similarity [J]. Journal of Visual Communication and Image Representation, 2015, 30: 117-124.
24. P. V. Sudeep, P. Palanisamy, C. Kesavadas and J. Rajan. Nonlocal linear minimum mean square error methods for denoising MRI [J]. Biomedical Signal Processing and Control, 2015, 20: 125-134.

A Novel Design of High-Throughout Hard Ware Implementation for Video Decoding based on H.264

Yi Wang[1,2], Xiuqin Su[1]

[1] Key Laboratory of Ultrafast Photoelectric Diagnostics Technology, Xi an Institute of Optics and Precision Mechanics of CAS, Xi'an, China
[2] University of CAS, Beijing, China

Corresponding author is Yi Wang

Abstract
In this paper, a novel high-throughput implementation for video decoding based on H.264 is proposed to improve the decoding efficiency. H.264 provides many new functions than previous video coding algorithm that bring more complex computations, Therefore, How t implementation of the decoder efficiency becomes a challenging. Research shows in the decoding flow there are many data dependency among different symbols. Especially in the entropy decoding this dependence is most obvious. Thence the CAVLC decoder requires large computation